Atmos. Chem. Phys. Discuss., 9, 11005–11050, 2009
www.atmos-chem-phys-discuss.net/9/11005/2009/

Atmospheric Chemistry and Physics Discussions

This discussion paper is/has been under review for the journal *Atmospheric Chemistry and Physics (ACP)*. Please refer to the corresponding final paper in *ACP* if available.

Uncertainties in atmospheric chemistry modelling due to convection and scavenging parameterisations – Part 1: Implications for global modelling

H. Tost[1,2], **M. G. Lawrence**[1], **and P. Jöckel**[1]

[1]Atmospheric Chemistry Department, Max Planck Institute for Chemistry, P.O. Box 3060, 55020 Mainz, Germany
[2]EEWRC, The Cyprus Institute, Nicosia, Cyprus

Received: 13 February 2009 – Accepted: 20 April 2009 – Published: 5 May 2009

Correspondence to: H. Tost (tost@mpch-mainz.mpg.de)

Published by Copernicus Publications on behalf of the European Geosciences Union.

Abstract

Moist convection in global modelling contributes significantly to the transport of energy, momentum, water and trace gases within the troposphere. Since convective clouds are on a scale too small to be resolved in a global model their effects have to be parameterised. However, the whole process of moist convection and especially its parameterisation are associated with uncertainties. In contrast to previous studies we address the impact of convection on trace species by examining simulations with five different convection schemes, rather than neglecting the convective transport for some or all compounds. This permits an uncertainty analysis due to the process formulation, without the inconsistencies inherent in entirely neglecting deep convection or convective tracer transport for one or more tracers.

Both the simulated mass fluxes and tracer distributions are analysed. Investigating the distributions of compounds with different characteristics, e.g., lifetime, chemical reactivity, solubility and source distributions, some differences can be attributed directly to the transport of these compounds, whereas others are more related to indirect effects, such as the transport of precursors, chemical reactivity in certain regions, and sink processes. The shorter-lived a compound is, the larger the differences and consequently the uncertainty due to the convection parameterisation, i.e., reaching up to ±100% for short-lived compounds, whereas for long-lived compounds like CO or O_3 the mean differences between the simulations are less than 25%.

1 Introduction

Moist convection plays an important role in the transport of energy and moisture in the lower atmosphere, where it is a substantial part of global circulation patterns, e.g. the Hadley and the Walker Cells. Furthermore, it contributes crucially to the vertical mixing of the troposphere, especially with respect to atmospheric trace species. Whereas the transport time required to go from the Earth surface into the upper troposphere

ACPD

9, 11005–11050, 2009

or vice versa is several days in the large scale motion flows, the high vertical velocities in up- and downdrafts within deep convective cells can substantially shorten this time to a few hours. In global modelling of the circulation and chemical composition of the atmosphere, these convective clouds can currently not be explicitely resolved with the state-of-the-art models, rather moist convection is parameterised. This leads to uncertainties in the description of the processes associated with cumulus convection (Arakawa, 2004). The main goal of most of these parameterisations is to "adjust the energy and water budget of a model column to achieve a more stable state of the atmosphere". A variety of parameterisations for moist convection in the atmosphere exists, some following similar concepts, and some with rather different approaches (e.g. Arakawa and Schubert, 1974; Kuo, 1974; Tiedtke, 1989; Hack, 1994; Zhang and McFarlane, 1995; Emanuel and Zivkovic-Rothman, 1999; Donner et al., 2001; Bechtold et al., 2001; Lin and Neelin, 2002; Nober and Graf, 2005). However, a "best" parameterisation cannot be identified easily in GCMs, since the main goal noted above is fulfilled by most of the schemes at least from a climatological point of view. Even though moist convection is an important aspect of numerical weather prediction, the uncertainties for this application are different than those in global modelling, i.e., the focus is more on the exact location and timing of a convective event.

For atmospheric chemistry the convection scheme is of additional importance, since not only energy and water are redistributed by convection, but also chemical constituents (greenhouse gases, pollutants, aerosols, etc.). The uncertainty associated in the parameterisation formulation of convection has been investigated in Tost et al. (2006b), but restricted to temperature, moisture, and precipitation and in a follow up study (Tost et al., 2007b) focusing on lightning and associated NO_x emissions. Several studies have attempted to address the influence of convection on the chemical composition of the atmosphere by excluding the convective transport of all or specific trace gases. One of the first examples was Lelieveld and Crutzen (1994), in which it was found that the O_3 lifetime is strongly influenced by convection. In a follow up study, Lawrence et al. (2003) found a larger effect due to the transport of ozone pre-

ACPD
9, 11005–11050, 2009

cursors, especially NO_x, than to the transport of O_3 itself, while other precursors, e.g., isoprene and its degradation products, have been found to be of similar importance in another study (Doherty et al., 2005). For short lived tracers, investigated with the chemically inactive compound ^{222}Rn, Mahowald et al. (1997) found that the neglect of convective transport leads to a substantial reduction of its mixing ratio by ≈ 50% in the upper troposphere. However, as shown by Lawrence and Salzmann (2008), the approach of comparing simulations with and without convective tracer transport will only capture part of the effect of deep convective transport, and will therefore fail to give a proper quantification of the effects that are caused by convection in general. An alternate approach is to examine the uncertainty in the process of convective transport and its effects on chemistry by employing a variety of cumulus parameterisations. Thus far, only Zhang et al. (2008) have employed this approach, focusing on the influence of the convection parameterisations on radon, finding differences of the order of 50% between several simulations-interestingly, of the same order as the differences found by Mahowald et al. (1997), in which convective transport was turned off entirely. In this study, we take this research a significant step further, by examining the effects of convective transport on atmospheric chemistry, using a variety of convection schemes, and including the calculation of atmospheric chemistry in both gas and aqueous phase.

2 Model description and simulation setup

2.1 Model description

In the present study the ECHAM5/MESSy atmospheric chemistry model (EMAC, Jöckel et al., 2006) is applied to investigate the influence of convection parameterisations on atmospheric trace species. EMAC consists of an atmospheric climate model, which is the 5th generation European Centre Hamburg general circulation model (ECHAM5, Roeckner et al., 2006) and the Modular Earth Submodel System (MESSy, Jöckel et al., 2005) to simulate tropospheric and middle atmosphere pro-

ACPD
9, 11005–11050, 2009

cesses and their interaction with oceans, land and human influences. In this study the standard convection parameterisation of Tiedtke (1989) with the modifications of Nordeng (1994) has been augmented by an interface allowing several other convection schemes to be implemented in parallel (Tost et al., 2006b). To determine the meteorology and the chemical composition of the atmosphere the MESSy submodels according to Table 1 have been applied. Five simulations with a similar configuration have been performed, differing only by the choice of the selected convection parameterisation. This study is based on previous work, in which the influence of the convection parameterisation on the large scale circulation and the hydrological cycle has been investigated (Tost et al., 2006b; Tost, 2006). The uncertainty in the lightning distribution based on the convection parameterisations has been discussed in Tost et al. (2007b). Due to those findings the lightning scheme that offers most robustness, i.e., a cloud top height dependent parameterisation (Price et al., 1997) is applied in this study. The associated NO_x emission is scaled to produce ≈4 Tg(N)/yr globally from flashes.

To compare the tracer transport using the different convection schemes a ConVective tracer TRANSport (CVTRANS) algorithm based on Lawrence and Rasch (2005) following the bulk approach ("leaky pipe") has been implemented. It is equipped with an interface to collect the required updraft and downdraft air mass fluxes and the respective entrainment and detrainment rates of the convection parameterisations. If required it applies an adjustment of these fluxes to guarantee positive definiteness, monotonicity and mass conservation such that the basic equation for updrafts (subscripted "u") and downdrafts (subscripted "d") is fulfilled [1]:

$$F_u^k = F_u^{k+1} + E_u^k + D_u^k \qquad (1)$$
$$F_d^{k+1} = F_d^k + E_d^k + D_d^k.$$

In this equation F_u^k and F_d^k denote the updraft and downdraft mass fluxes, and F_u^{k+1} and F_d^{k-1} the mass fluxes from the layer below and above. E_u^k and E_d^k are the entrain-

[1] An additional requirement for the convective tracer transport routine is that the downdrafts may not exceed the updraft, which is usually fulfilled, but otherwise an adjustment is performed.

ACPD
9, 11005–11050, 2009

ment and D_u^k and D_d^k the detrainment rates from the respective fluxes in this layer. All fluxes are in kg/(m^{2}s).[2] Finally the convective tracer transport in updrafts, downdrafts and the mass balancing subsidence is calculated independently[3] from the underlying convection scheme according to the following equation:

$$
\begin{aligned}
C^k = ((AM^k - (F_u^k - F_d^k + D_u^k + D_d^k) * \Delta t) * C^k \quad & (2)\\
\text{(unaffected by convection)}\\
+ (F_u^k - F_d^k) * \Delta t * C^{k-1}\\
\text{(subsidence)}\\
+ D_u^k * \Delta t * C_{ud}^k\\
\text{(detrained from updraft)}\\
+ D_d^k * \Delta t * C_{dd}^k)\\
\text{(detrained from downdraft)}\\
/AM^k .
\end{aligned}
$$

The first term determines the fraction of the mixing ratio C^k in a specific layer which is not affected by the convection, the second the effects of the mass balancing subsidence from the layer above (index $k-1$), the third the fraction of detrained species from the updraft with mixing ratio C_{ud}^k, and the fourth term fraction of detrained species from the downdraft with mixing ratio C_{dd}^k, with AM^k being the airmass per unit area in that grid cell.

The scavenging scheme described in Tost et al. (2006a) has been extended to additionally allow uptake of species onto ice surfaces, the sedimentation of the crys-

[2]Note that the mass fluxes are defined at the interfaces, e.g., F_u^k is the mass flux at the upper boundary of the grid box, whereas the entrainment and detrainment rates are defined as grid box mean values.

[3]The mass fluxes and entrainment and detrainment rates are taken from the convection parameterisation.

tals, i.e., a slow vertical downward transport, the release from the evaporating ice crystals and the transition of species into the liquid phase during melting processes. For the uptake/equilibrium purpose an iterative Langmuir-uptake formulation following the approach of Tabazadeh et al. (1999) has been applied. In this study only HNO_3 is considered for the uptake onto ice particles. The influence that the additional ice uptake of HNO_3 has on O_3 is relatively small (of the order of a few %), but for HNO_3 the uptake results in a reduction of up to 30% in the upper troposphere (as shown in the supplement http://www.atmos-chem-phys-discuss.net/9/11005/2009/acpd-9-11005-2009-supplement.pdf), in agreement with previous calculations (von Kuhlmann and Lawrence, 2006).

2.2 Simulation setup

In this study five simulations have been performed with different convection parameterisations, according to Table 2. More details about the schemes and their implementation in the model are described in Tost et al. (2006b). In contrast to the previous studies with this model,the convection schemes have been "tuned" to achieve both realistic radiation and precipitation fluxes compared to NOAA and ERBE (radiation) and CMAP (precipitation) fluxes within the uncertainty range of these values (see supplement).

A time period of four months is calculated, from 1 September 2005 to 1 January 2006. During that special period two aircraft campaigns took place which are analysed in detail in an accompanying publication, whereas this study focuses on global implications. The meteorology is "nudged" (Newtonian relaxation) towards the temperature, surface pressure, divergence and vorticity from ECMWF analysis data to achieve the same large-scale weather patterns. There are no direct feedbacks between chemical species and meteorology (no variable radiative transfer forcing through O_3 or other trace gases); therefore the different tracer distributions are caused by the convection schemes. However, since water vapour changes due to the choice of the convection scheme, the chemistry is directly influenced by those changes, e.g., through OH production from H_2O. The model is applied at a resolution of T63 (i.e., with a triangular

ACPD
9, 11005–11050, 2009

spherical truncation corresponding to a quadratic Gaussian grid of ≈1.875 by 1.875 degrees in latitude and longitude) with 87 vertical hybrid pressure levels up to 0.01 hPa.

3 Results

3.1 Global mass fluxes

A major part of the vertical redistribution of trace species in the troposphere is caused by the overturning of air in the convective systems. Consequently, the global convective mass fluxes, which cannot be measured well, are an indicator for the strength of the vertical transport of constituents. Since within one model column the air mass is conserved, convection leads only to a redistribution of tracers (due to combined updraft, downdraft and subsidence mass fluxes). The zonal average updraft mass fluxes (time average over the 4 month simulation time) with the different convection schemes are shown in Fig. 1.

In all the simulations the deep convection of the tropics is evident, reaching almost up to the tropopause. The two-peak shaped distribution in the tropics is caused by the overlay of the ITCZ in the Atlantic and the Pacific (and the corresponding shifts in latitude) in addition to the intense convection in the South Pacific Convergence Zone (SPCZ). Furthermore, in addition to the almost zonally omnipresent shallow convection, enhanced deep convective activity is calculated in the midlatitude storm tracks.

However, both the absolute strength of the convection (in terms of mass fluxes) and also the average convective cloud top height (and consequently the outflow height) depend strongly on the selected convection schemes, e.g., the overall strength in the EC simulation is much larger than in all others (with an even more enhanced shallow convective fraction), whereas EMA and B1 show weaker overall convective activity. This is partly a consequence of the applied "tuning" mentioned above, since the radiation balance can be perturbed with increasing convective activity. This aspect will be discussed in more detail below. ZHW and B1 are characterised by the deepest con-

ACPD
9, 11005–11050, 2009

vective activity with substantial mass fluxes up to 200 hPa or even higher. In contrast, T1 convection generally peaks a little lower, especially in the extra-tropics. EC, EMA, ZHW, and B1 hardly calculate convection in the polar regions, in contrast to T1. The average profiles (temporally and spatially averaged) in Fig. 1f show the shallow convection (below 750 hPa) with a substantial strength, as noted above, most pronounced in EC. Above, the mass fluxes decrease monotonously in nearly all simulations. However, EMA, ZHW and B1 show a larger mass flux than T1 and EC at 300 hPa, causing a steeper gradient in the mass fluxes for the latter two cases and therefore resulting in a weaker transport into the upper troposphere. ZHW even shows a small increase in the mass flux, which is mainly caused by the activation of the Hack (1994) part of the scheme (local instabilities which are in the other simulations are stabilised by the large-scale cloud scheme (compare Tost et al., 2006b).

Even though the mass fluxes are different in all the simulations, in none of them is a significant mass flux over the tropopause computed, i.e., the overshooting events injecting air mass and consequently tracers into the stratosphere are almost negligible, comparable to the findings of Lelieveld et al. (2007). The corresponding downward mass fluxes (displayed in the supplement http://www.atmos-chem-phys-discuss.net/9/11005/2009/acpd-9-11005-2009-supplement.pdf) also show different spatial distributions, but are of similar strength, within about a factor of two, in all simulations. Especially in the EMA simulation, the downdrafts are weaker in the upper troposphere, causing a slower downward transport of trace species from the UT region. Since the updrafts are balanced by the downdrafts and the mass balancing subsidence (see Eq. 3), the overturning time is shorter in the simulations with smaller mass fluxes (both upward and downward). In combination with the chemical lifetime this has implications for the vertical distribution of tracers.

3.2 Tracer distributions

In the real atmosphere chemistry has a major influence on many trace species. Chemical reactions can mask the differences in transport, but can also amplify those signals.

Furthermore, scavenging, liquid phase reactions, and downward transport in hydrometeors (and their potential re-evaporation and subsequent release of species) have an additional impact on the trace species budgets. Since the latter process depends on liquid and frozen water (clouds and precipitation), which are determined differently in the individual convection schemes, these contribute substantially to the differences in the vertical distributions of many compounds. Therefore, in the following sections, first chemically inactive tracers are analysed to understand the different transport characteristics, followed by an analysis of chemically reactive and partly soluble compounds to see the implications of the transport. It is not the aim of this study to decide which convection scheme is best in reproducing the observed state of the atmosphere, but to highlight the differences and uncertainty caused by the convection parameterisations. The analysis whether the schemes are suitable for simulating a stable atmospheric state has been done by Tost et al. (2006b) and a comparison with observations from two specific field campaigns will be presented in an accompanying publication.

3.2.1 Chemically inactive tracers

(a) H_2O:
Water vapour is the driving force for moist convective activity, therefore the differences in moisture distribution caused by the convection schemes are relevant for addressing the uncertainty due to the convection parameterisation in an atmospheric chemistry general circulation model. In the current setup the chemical contribution to H_2O is neglected: the chemical production of H_2O from CH_4 oxidation (relevant mostly for the stratosphere) is prescribed as a climatological tendency. Furthermore, H_2O is not consumed by chemical reactions. However, the meteorological feedbacks (radiation and the hydrological cycle) from the deep convection parameterisation cannot be eliminated due to their close relationship to the convective dynamics.

Figure 2a depicts the zonal mean H_2O mixing ratio in the T1 simulation, with highest values at the surface in the tropics and and decreasing values poleward and upward. Comparing the global mean profiles for the simulation period, substantial absolute dif-

ferences above the boundary layer up to an altitude of ≈400 hPa can be seen, with EC simulating the moistest and B1 the driest atmosphere (Fig. 2b). The relative differences $(100 \cdot (X - T1)/T1)$ between the individual simulation and the T1 simulation are depicted in the panels c to f of Fig. 2. Note that the largest differences occur in the regions with lowest absolute values, being therefore not necessarily relevant for climate [4]. In the EC simulation the whole troposphere above 850 hPa is moister than in the reference simulation, in agreement with an enhanced integrated water vapour (IWV) as shown in Tost et al. (2006b). This results in an atmosphere that can be more easily destabilised and consequently more frequently convection is triggered. That is in agreement with the stronger convective updraft mass fluxes (see Fig. 1f). The enhanced moisture, being most dominant in the upper tropical troposphere results from both the stronger convective activity and the detailed treatment of an ice phase in the convective microphysics scheme. However, the absolute values of the H_2O are sensitive to the convective precipitation formation rate (conversion rate of convective cloud water into convective precipitation, a parameter of the convection scheme). Nevertheless, the selected values show a good agreement between observed outgoing long-wave radiation (OLR) and precipitation rates. The water vapour distribution in the EMA simulation is characterised by more regional differences. In the tropical and subtropical middle and upper troposphere the atmosphere is more humid, whereas it is drier in the extra-tropics and the lower troposphere. In particular, the region with the strongest convective updraft mass fluxes is characterised by less H_2O in EMA. Since the absolute strength of the convection is lower than in T1, there is a weaker moisture transport into the middle troposphere in that region. Furthermore, since there is less convective activity in the subpolar and polar regions, the upward moisture transport is also reduced, resulting in the drier atmosphere. Since the convective outflow height is higher compared to T1, more moisture is transported into the tropical tropopause layer and is subsequently transported downward in the Hadley Cell in both hemispheres. This forms the two

[4] However, they can be relevant for climate due to additional cloud formation (e.g., cirrus formation in the upper troposphere).

ACPD
9, 11005–11050, 2009

lobes in the subtropical subsidence regions. The difference in ZHW is characterised by a tri-polar structure: a drier lower troposphere in both the subtropics and the tropics, a moister mid to upper troposphere, and a drier uppermost tropical tropopause layer. A slightly weaker shallow convection, i.e., less efficient transport of moisture is likely to explain the drier lower troposphere, and the slightly more intense updrafts in the middle and upper troposphere can cause the mid and upper tropospheric moisture enhancement. The drier TTL is most likely caused by the frequent activation of the Hack part of the convection scheme, which lacks a detailed ice microphysics and overestimates the stabilising adjustment (compare Tost et al., 2006b). However, some of these arguments cannot be straightforwardly proven. The B1 simulation represents a drier atmosphere, and shows the strongest precipitation. Consequently, too much water vapour condenses, leading to lower H_2O mixing ratios in the lower troposphere. Additionally, the overall convective mass fluxes are lowest in this simulation, causing an overall weaker transport of moisture into the uppermost troposphere. Since H_2O is a primary source of OH ($H_2O+O^1D \rightarrow 2OH$), the main oxidant in the lower atmosphere, it also strongly impacts the oxidation capacity and influences almost all chemically reactive compounds.

For an evaluation of the water vapour columns we refer to Tost et al. (2006b).

(b) ^{222}Rn:

^{222}Rn is used as a standard tracer to analyse (continental) convection (Jacob and Prather, 1990) since it is chemically inactive, insoluble, but decays radioactively with a lifetime of ≈4.8 days These properties make it susceptible to transport alone, i.e. with its help it is possible to deduce the transport characteristics of the convection schemes. Furthermore, some indications for the differences in the convective cloud top and therefore the outflow height can be drawn from the analysis. The emission is set to 1 molecule/(cm·s) over land and zero over water and ice in this study.

However, only very few measurement data are available providing vertical profiles of ^{222}Rn. In a previous study (Tost, 2006) it was found that the vertical profiles differed

ACPD
9, 11005–11050, 2009

substantially when alternative convection schemes were applied, but were all within the large scatter of the measurement data. The zonal average distribution, depicted in Fig. 3a (note the logarithmic scale) for the T1 simulation is dominated by the land sea contrast between the Northern and Southern Hemisphere, resulting in higher mixing ratios between 10° N and 70° N. The tropical convection leads to elevated mixing ratios up to 600 hPa, whereas the convective activity in the northern hemispheric storm track is able to transport a larger number of ^{222}Rn atoms even up to 400 hPa. The global mean profile (see Fig. 3b) is quite similar for all the simulations, with only minor differences at ≈600 hPa and 300 hPa, with the exception of B1. The simulation using the Bechtold scheme shows a more pronounced C-shape profile with substantially lower values around 700 hPa, but elevated values in the upper troposphere (above 500 hPa, most pronounced at ≈350 hPa). Furthermore, the mixing ratios in the boundary layer are slightly higher than in the other simulations. Consequently, in this simulation the transport of radon from the boundary layer into the troposphere is enhanced, particularly since it is less mixed with entrained air from the mid troposphere. This is supported by the results of Fig. 1, which showed some convective activity, but not the strongest mass fluxes due to a weaker entrainment.

The relative differences to the T1 simulation in the zonal mean distribution of ^{222}Rn (Fig. 3c–f) exhibit a more complicated picture than the global mean profile. The EC simulation is characterised by lower mixing ratios in the tropical lower troposphere, but elevated mixing ratios in the tropical middle and upper troposphere. This can also be explained with the help of Fig. 1a and b, since the shallow convection is stronger in EC, transporting more tracer-rich air from the surface to the mid and upper troposphere. At the tropopause (black line) and above, the absolute mixing ratios become very small, so that large relative differences are not necessarily significant. It is important to consider not only the differences in the convective regions but also in the subsidence regions, since a more efficient and faster transport into the upper troposphere can lead to higher mixing ratios in regions that are not directly influenced by the convective activity, but also by horizontal transport. In particular, differences occur in regions around 20° to

ACPD
9, 11005–11050, 2009

30° N, where no significant convective updrafts are simulated. These can result from the faster overturning within the Hadley Cell driven by the convection. Farther away from the tropics the differences are likely not significant, since the lifetime of ^{222}Rn is too short to be uplifted in the tropics and then transported into those regions. The differences between T1 and EMA (Fig. 3d) are smaller compared to the other simulations. Even though the total convective updraft mass fluxes are much lower than in T1, the zonal mean distribution is not lower everywhere, but shows some enhanced values in the tropical mid troposphere. The less intense shallow convection in EMA leads to lower values in the tropical boundary layer, but in the upper troposphere T1 is characterised by higher values than EMA due to more intense convection in the tropical updraft regions. In the extra-tropics the convective mass fluxes are weaker, therefore the upward transport of ^{222}Rn is less efficient. In the tropics the downdrafts are substantially weaker in EMA compared to T1 (see the electronic supplement), resulting in reduced downward transport and consequently slightly enhanced mixing ratios in EMA above the downdraft region at ≈600 hPa. In ZHW the mid and the upper troposphere are characterised by enhanced radon mixing ratios compared to T1. The upper tropospheric enhancement is likely being caused by the deeper convection simulated with ZHW. Furthermore, the gradient of the updraft mass fluxes is less steep in ZHW, leading to a more vigorous transport into the upper troposphere. As already discussed for the global mean profile, the Bechtold scheme causes a more C-shape like profile, with lower values than T1 in the mid troposphere, but substantially enhanced mixing ratios of radon in the upper troposphere compared to the other simulations, especially in the tropics. This is caused by the weaker mixing with mid troposphere air, and can become very important for chemical conversion (in terms of surrounding conditions like temperature, radiation and photolysis, etc.).

Most of the atmospheric ^{222}Rn is located in the troposphere; however the choice of the convection scheme alters the fraction reaching the upper troposphere, whereas the total atmospheric burden is similar in all simulations since it depends only on the amount that enters the stratosphere, which is small due the short decay time. Table 3

ACPD
9, 11005–11050, 2009

depicts the upper tropospheric burden (500 hPa to the tropopause) and the fraction of the total atmospheric radon burden. The difference in the burden exceeds 40% between the B1 (highest value) and the Ema simulation (lowest value). Furthermore, a substantially larger fraction of the total atmospheric ^{222}Rn is located between the 500 hPa and the tropopause level in the Bechtold simulation, reaching up to 22.6%. The fraction for the other schemes is quite similar. This additionally supports enhanced transport of boundary layer air which is enriched in radon into the upper troposphere using the Bechtold scheme. Except for the B1 simulation, the total upper tropospheric burden does not depend substantially on the selected convection parameterisation. The spatial differences however are of a similar magnitude as found by Zhang et al. (2008). Overall, even though the distribution of the ^{222}Rn mixing ratios is similar with the different convection schemes (with a slight exception of the Bechtold scheme), the absolute values can vary by up to a factor of two.

3.2.2 Chemically active tracers

In this section, a selection of species with different chemical lifetime, reaction pathways, and solubility are analysed.

(a) CO:
CO has a relatively long lifetime and is therefore suitable for addressing questions of convective and long range transport. However, in contrast to ^{222}Rn it is not chemically inactive, but is oxidised mainly by OH. Consequently, the carbon monoxide mixing ratio is also dependent on the OH distribution, which is dominated by local processes and the water vapour concentrations (see above). The zonal average mixing ratio of CO in the T1 simulation is presented in Fig. 4a. Since most of the emissions are anthropogenic, the maximum is located in the Northern Hemisphere, with some biomass burning contribution in the tropics. The zonal average distribution looks comparable

ACPD
9, 11005–11050, 2009

to that of radon[5]. The winter hemisphere shows a well mixed CO distribution due to the extended lifetime caused by the reduced wintertime OH production, but enhanced carbon monoxide is also simulated in the tropical tropopause layer, transported there mainly by convection. The global mean profile of CO (see Fig. 4b) is similar in all simulations: a slight increase in the boundary layer and a slow decrease up to almost 300 hPa, followed by a strong decrease up to 50 hPa. Above that, the stratospheric source of CO by photodissociation of CO_2 causes a strong increase in the carbon monoxide mixing ratios. However, some differences are obvious: for example, the EC simulation shows the lowest CO mixing ratios. This is consistent with the enhanced H_2O mixing ratios, leading to an enhanced OH production and consequently a decrease in the CO lifetime. On the other hand, B1 shows a slightly different shape; comparable to the ^{222}Rn profiles a more distinct C-shape profile can be seen, resulting from a more efficient direct input of lower tropospheric CO enriched air into the upper troposphere and a less efficient mixing with air from the mid troposphere. Analysing the relative differences of the zonal mean carbon monoxide mixing ratios between the simulations (Fig. 4c–f), some zonal patterns appear. Even though CO is in general lower in EC, it is enhanced in the northern branch of the main convectively active zone (0° to 20° N) in the middle and upper troposphere. Due to a relatively uniform change in H_2O and OH this is not likely an effect of chemistry alone, but of the convective transport characteristics. The enhanced updraft mass fluxes cause a more vigorous transport to higher altitudes. However, this is partly contradictory, since it occurs only in the Northern Hemisphere, even though the convective activity is similar in both hemispheres. An aspect to consider is the availability of OH reaction partners. In the Northern Hemisphere with stronger pollutant emissions the available hydroxy radical (which has a lower production rate in the winter hemisphere) is effectively scavenged by the other available pollutants. In the tropical regions, the positive feedback between CO and OH results in a strong enhancement in CO, given its substantial emissions from biomass

[5]Note that the scale is linear for CO.

burning, accompanied by a reduction in the available OH (which is further reduced due to reactions with various hydrocarbons), whereas in the Southern Hemisphere the long-lived CO is the only significant OH reaction partner, resulting in the higher OH levels and the substantial reduction of CO mixing ratios over the southern hemispheric oceans.

The slightly weaker convection in the EMA simulation leads to slightly higher values than the reference simulation close to the surface in the tropics, and consequently reduced values in the convective updraft and outflow regions. However, all the changes are in the range of a few % only, and therefore not significant and they cannot easily be attributed to the alternative convection parameterisation alone. In fact, it is also likely that they are a potential result of the spreading of other differences in the model (due to its non-linearity, discussed below).

The ZHW simulation is characterised mostly by slightly enhanced CO mixing ratios compared to T1, except for the tropics, and there especially in the southern lobe of the convective mass fluxes. The pattern appears to be different from the differences in the moisture (as well as the differences in OH itself, which is shown in the electronic supplement), ruling out the possibility that OH is responsible for that pattern, leaving it mainly to transport. However, also in this simulation the relative differences are quite small.

In contrast to this, the B1 carbon monoxide distribution shows larger differences. The reduced values in the lower tropical troposphere and the enhanced CO in the upper troposphere can be attributed to a direct input of almost undiluted, CO rich air into the upper troposphere by convection. Since there is hardly interaction with the lower to mid troposphere, detrainment of CO is of minor importance. Additionally, the reduced moisture causes a slightly reduced OH production, and therefore extends the CO lifetime, resulting in enhanced mixing ratios in the upper troposphere. Horizontal transport strongly influences the distribution, including subsidence into the subtropical regions and transport across the tropopause in the midlatitudes. The influence of the convection parameterisation on CO is limited due to its long lifetime, so that all relative

ACPD
9, 11005–11050, 2009

differences are in the range of a maximum of ±20%. Furthermore, the indirect effects via the modified lifetime due to changes in OH are of similar importance.

Since the CO distribution has been in slightly underestimated with the standard convection scheme of EMAC (T1) as shown by Pozzer et al. (2007), the higher values of the mean profile of all other schemes tend to push the model towards the right direction improving the agreement. Since there are no major changes in the general shape of the profile, the agreement in terms of correlation and standard deviation is similar with all convection schemes.

(b) HCHO:

Formaldehyde is chosen as an exemplary species that is chemically more reactive than CO. The distribution is dependent on the convective transport of precursors and the compound itself, but additionally it is moderately soluble. Therefore, scavenging and subsequent rainout play a significant role for the global patterns adding the dimension of uncertainty of the convection schemes in cloud and precipitation water. The zonal average distribution for the reference simulation is depicted in Fig. 5a. The highest values occur in the tropics and subtropics, near the surface due to the enhanced hydrocarbon emissions from both natural (isoprene) and anthropogenic (propane, butane) sources and their subsequent degradation. With increasing altitude the photolysis gains in importance in the destruction of HCHO, causing the decrease in the mixing ratios. Comparing the global mean profiles (Fig. 5b), all simulations show a similar distribution, with only B1 having significantly smaller values in the mid troposphere and an enhancement at ≈400 hPa. Therefore, it is astonishing how large the relative differences between the simulations are: up to ±50%, as depicted in Fig. 5c–f. The EC simulation has higher values of HCHO mainly in the middle and upper troposphere due to the enhanced OH (as seen in the supplement), which causes faster degradation of hydrocarbons into formaldehyde. The lower values in the tropical tropopause region correlate well with low OH values in the same region (always compared to the reference T1). However, in the lower troposphere lower values than in T1 are calculated.

ACPD
9, 11005–11050, 2009

Since the convective mass fluxes are stronger in this area, the enhanced convective transport leads to an additional enhancement of HCHO in the middle troposphere, and consequently a reduction in the boundary layer. This effect outweighs the chemical effects, since these patterns are different in OH and HCHO. Furthermore, the precipitation in ECMWF is less intense in the tropics, causing a weaker downward transport of HCHO within hydrometeors and their subsequent release due to evaporation and the lower solubility at high temperatures.

The EMA simulation shows only minor differences to the reference (Fig. 5d): a slight enhancement at the surface, lower values in the tropical lower troposphere, an enhancement in the tropical mid troposphere, lower values from 500 to 300 hPa and enhancement again in the tropopause region. As for EC this distribution partly correlates with the differences in OH, but this alone is not sufficient to explain all the differences. Since the convection reaches on average higher, the larger values in the upper troposphere around the tropical tropopause are caused partly by the convective transport of near surface air with enhanced formaldehyde mixing ratios into that region. Due to the moderate solubility not all of the HCHO is scavenged, but can reach higher altitudes. Since the main detrainment is at a higher altitude than in T1 (in this simulation between 500 and 300 hPa), this shift is also one reason for the dipolar pattern in the upper tropical troposphere.

ZHW is characterised by an enhancement in the mid to upper troposphere (mainly in the tropics) and a substantial decrease directly at the tropical tropopause. In this simulation the two enhancements occur mainly in the two major convective detrainment regions (the regions where the convective updrafts show the strongest gradients, compare Fig. 1d). The higher values between 500 and 300 hPa again correlate well with the OH enhancement (see supplement). However, the strong decrease of HCHO at the tropical tropopause cannot be explained easily. Even though OH has lower values in ZHW compared to T1, the effect is less significant. In spite of convection not being active at this altitude, a similar feature is detected for CO and also ^{222}Rn, the latter being only influenced by transport. One possible explanation is that the convection parame-

ACPD
9, 11005–11050, 2009

terisation causes indirect effects in terms of transport, i.e., changes in the large-scale motion which can lead to a shift in the zonal average distribution. The B1 simulation shows again the typical behaviour for this setup, caused from the convective transport (also obvious in the global mean profile): a decrease in mid troposphere mixing ratio and and enhancement in the upper tropical troposphere due to almost undiluted upward transport of boundary layer air which is rich in HCHO up to the tropopause. The correlation to the OH distribution is low, indicating that transport is the dominant reason for this pattern.

Pozzer et al. (2007) report a small high bias for HCHO; since the T1 simulation has usually the highest value in the mean profile, the other schemes also tend to go into the right direction. Only the B1 scheme, with the significantly lower values in the lower to mid-troposphere seems to have too low values.

(c) HNO_3:

For the distribution of nitric acid another aspect has to be considered in addition to convective transport of HNO_3 and its precursors, chemistry, scavenging and wet deposition: namely the uptake on ice particles. Depending on the detailed treatment of cloud and precipitating ice in the convection parameterisations this yields yet another source of uncertainty related to the convection scheme. Furthermore, in contrast to ^{222}Rn or HCHO the burden increases by more than an order of magnitude at the transition into the stratosphere. The zonal mean distribution of the reference simulation (Fig. 6a) shows enhancements of nitric acid at the surface between 20° N and 40° N due to anthropogenic, industrial NO_x emissions. A second region with enriched HNO_3 is located around the equator (10° S to 10° N), caused by NO_x emissions from biomass burning and lightning. The low values in the upper troposphere are caused by the uptake on ice crystals (see supplement http://www.atmos-chem-phys-discuss.net/9/11005/2009/acpd-9-11005-2009-supplement.pdf). The global mean profiles show a relatively similar shape (S-like) for all simulations, with EMA having highest values in the boundary layer and EC mainly in the mid troposphere. However, in the global aver-

ACPD
9, 11005–11050, 2009

age the differences are relatively small. Therefore, it is surprising that the differences in the zonal mean are as high as 100%. However, it has to be considered that these large relative differences occur in regions in which the absolute values of HNO_3 mixing ratios are relatively low. Analysing the differences between EC and T1 (Fig. 6c), the largest differences occur in the mid latitudes and polar regions. In T1 convection is active in those regions as well (i.e., convective updraft mass fluxes are calculated) and due to the cold temperatures and the simplified treatment of the ice phase in the T1 convection, the sink by scavenging on ice is stronger. Furthermore, the precipitation is lower in EC than in T1, and thus the scavenging by liquid precipitation is enhanced in T1. Since in these regions the absolute values of the HNO_3 mixing ratio are small, the relative differences quickly reach high values. A different aspect is seen in the tropics. In the Southern Hemisphere EC calculates lower values than the reference due to more vigorous shallow convection (up to 600 hPa) and associated rainfall and subsequent wet deposition. However, at $\approx 10^{\circ}$ N EC simulates significantly enhanced HNO_3 mixing ratios. This results partly from a different distribution of the convective cloud water and subsequent precipitation formation which is much weaker in the EC simulation. Due to the resulting reduced scavenging in this region, the nitric acid mixing ratio is higher.

The EMA simulation is characterised by enhanced HNO_3 in the boundary layer in the lower hemisphere and higher nitric acid mixing ratios up to 600 hPa in the Northern Hemisphere. Above that, a lower HNO_3 content than in T1 is simulated up to the tropopause. In the tropopause layer more HNO_3 is calculated in EMA, since the oxidant level is higher, leading to a more rapid conversion of NO_x into nitric acid as in T1. ZHW has a quite similar distribution in the tropics with slightly lower values, but HNO_3 enhancement in the midlatitude storm tracks. This results mainly from the precipitation distribution: in the tropics a slight overestimation of rainfall (compared to CMAP (Xie and Arkin, 1997)) over the continents leads to a too efficient scavenging of nitric acid (originating from biomass burning NO_x), whereas the precipitation in the storm tracks is underestimated, causing too weak rainout.

The B1 simulation has mainly lower values in the tropics, except around 5° N at the

ACPD
9, 11005–11050, 2009

surface, but enhanced HNO_3 mixing ratios in the midlatitude to polar regions.

In comparison to the findings of Jöckel et al. (2006) where a tendency to underestimate the nitric acid mixing ratio in the lower and overestimate it in the upper troposphere the tendency of most schemes has been diagnosed, especially the Ema simulation appears to be most suitable to overcome these issues. However, since the uptake of HNO_3 on ice has been neglected in Jöckel et al. (2006) this effect can counterweight the effect of the convection schemes.

(d) O_3:

Ozone has been selected as a compound in which all of the effects are combined, mainly through the indirect effects on the precursors. The zonal mean ozone distribution is presented in Fig. 7a for the T1 simulation. The tropospheric patterns are characterised by the vertical gradient towards the higher values in the stratosphere with a more efficient downward transport in the subtropical subsidence regions. The upper tropospheric O_3 distribution is dominated by a large fraction by the stratosphere-troposphere transport, which might also be affected to a lesser degree by the choice of the convection parameterisation. In the Northern Hemisphere local production contributes to the enhanced O_3 mixing ratios at the surface, causing the asymmetric shape of the ozone mixing ratio distribution, which was evaluated in detail in Jöckel et al. (2006). The global average profile (Fig. 7b) looks similar for all the simulations, all capturing the strong increase in O_3 near the tropopause. However, in the mid troposphere a spread of $\approx$5 ppb exists between EMA (lowest values) and B1 (highest ozone mixing ratios). Furthermore, typical features of convective transport in clean, remote regions, e.g., an upper tropospheric minimum due to lifting of ozone poor air from the surface are absent in all global mean profiles, and consequently only of local importance. The differences between the simulations with the alternative convection schemes to the reference in Fig. 7e–f cannot be explained easily.

EC has reduced values in the tropical updraft at the equator, but slightly enhanced values in the northern midlatitudes. The shift in patterns around the tropopause is likely

to be explained by the different moisture distribution, as well as a different stratosphere-troposphere exchange. EMA, having lower values in the southern updraft branch in the mass fluxes, also shows lower O_3 values in that region. Since the absolute values of ozone have a minimum at the tropical surface, this is an indirect effect of a less efficient transport of precursors into the mid troposphere. In the upper tropospheric winter hemisphere the changes are also likely related to indirect, i.e., chemical effects, such as the change in the oxidising efficiency of the atmosphere due to altered chemical oxidant distributions due to the absence of strong deep convective activity in both EMA, and T1 simulations. Since ZHW has a mass flux distribution that is similar to T1, the relative differences likely have their origin in the chemical effects. However, the reduction in the equatorial mid troposphere coincides with the enhancement in ^{222}Rn (compare Fig. 3e). Further upward the opposite effect occurs, i.e., an enhanced ozone production or a reduced ozone loss. Additionally, there is a stronger inflow of O_3 from the stratosphere in the midlatitudes, which is more pronounced in the Southern (summer) Hemisphere.

The B1 simulation shows a completely different picture: O_3 is enhanced in the mid and the upper troposphere, and this phenomenon is not only limited to the tropics, where convection has the strongest impact, but is spread all over the troposphere. However, in the tropics the differences to T1 are largest. The maximum in the upper tropical troposphere (UT) results from the direct transport (see above) of boundary layer air into the UT, where O_3 production is stronger due to enhanced ozone precursors. The lower OH additionally reduces one of the O_3 sink processes ($O_3+OH \rightarrow O_2+HO_2$). The enhancement in the lower troposphere compared to T1 is the result of both convective transport and chemical effects. Since O_3 has an intermediate lifetime in the troposphere, the transport of the compound and also of its precursors influence the ozone distribution. Additionally, changes in the chemistry have non-linear feedbacks that become visible in a compound like O_3 that is so dependent on multiple other species (see discussion below). Furthermore, even though ozone is not soluble, many of its precursors are strongly influenced by scavenging and rainout/washout

ACPD
9, 11005–11050, 2009

processes, which also contribute to the different patterns in the simulations.

Calculating the tropospheric ozone burden, the differences do not exceed a value of 8%, with highest value for the B1 and lowest for the EC simulation (compare Table 4). These differences are considerately smaller than the differences for ^{222}Rn noted earlier in Table 3.

These differences are all smaller than the range found in previous studies (Lelieveld and Crutzen, 1994; Lawrence et al., 2003; Doherty et al., 2005) completely neglecting the transport of ozone and/or its precursors, which are in the range of −20% to +12%.

In general, for O_3 the overall picture is too complex to directly associate specific patterns with physical and chemical processes. However, it can be seen that the choice of the convection parameterisation results in a non-negligible uncertainty of 5 to 25% in the zonal average ozone distribution.

Jöckel et al. (2006) did an extensive evaluation of O_3 in the atmosphere. Enhanced upper tropospheric values compared to the standard scheme, which tends to underestimate ozone at 400 hPa are mainly found using ZHW and B1. However, the tropospheric burden of all simulations are higher than calculated by Jöckel et al. (2006), except for EC which has the same value; consequently some improvement in the model formulation of processes, e.g. the HNO_3 uptake on ice result in slightly enhanced O_3 values.

3.3 Scavenging and wet deposition

The different convection schemes do not only cause different precipitation patterns (see Tost et al., 2006b and http://www.atmos-chem-phys-discuss.net/9/11005/2009/acpd-9-11005-2009-supplement.pdf), but also result in different vertical distributions of cloud and precipitable water. Consequently, the scavenging efficiency for trace gases and aerosols depends not only on the distribution of the species (due to the convective transport), but also on the condensed water and the precipitation regions. However, since the global precipitation distribution differs only within the range of uncertainty given in Tost et al. (2006b), the overall wet deposition looks relatively similar in all

simulations. Nevertheless, being the combined result of the tracer and the precipitable water distributions, some differences are evident.

Figure 8 depicts the differences in the zonal averages of the accumulated wet deposition of the two main acidifying compounds nitrate and sulphate. The general features are very similar (except for NO_3^- in ZHW), and are mainly caused by the climatologically realistic occurrence of precipitation and wet deposition therein. The total amount differs according to differences in the precipitation, e.g., since ZHW has almost everywhere lower precipitation, the total amount of wet deposition is lower. Detailed pictures of the location of the main differences can be found in the supplement (http://www.atmos-chem-phys-discuss.net/9/11005/2009/acpd-9-11005-2009-supplement.pdf). Nevertheless, stronger wet deposition does not necessarily mean lower atmospheric burden, since enhanced wet deposition can be compensated by reduced dry deposition and vice versa. The differences in the wet deposition are smaller than those in the tracer distributions since strong convective activity is characterised by both strong upward motion (vertical tracer transport) and strong precipitation (resulting in strong wet deposition). Consequently, for highly soluble compounds like nitrate the strong upward motion is largely compensated by the downward motion within the precipitation. Additionally, if the convective precipitation is not occurring in one specific grid box with one scheme, convective activity possibly occurs one time step later or in the adjacent grid box. Alternatively the precipitation is formed by the large-scale cloud scheme, also causing wet deposition and therefore wet deposition with only a slight shift in the patterns. For sulphate wet deposition the differences in liquid water cause different in-cloud sulphate production (also affected by the different oxidant distributions), and consequently with the combined effects on chemistry and cloud processes slightly larger differences can occur locally. On the other hand, for sulphate the source (i.e., the in-cloud sulphate formation) is more directly linked to the sink by wet deposition. Therefore, the zonal average distribution of SO_4^{2-} shows smaller differences for the ZHW scheme than for nitrate, since via cloud and precipitation formation both the source and the sink processes take place simulta-

neously.

In comparison with the observation data used in Tost et al. (2007a) the EC simulation agrees better in terms of correlation and linear fit than the T1 simulation for both NO_3^- and SO_4^{2-}. For sulphate all other simulations show a higher correlation than T1 for the selected stations. Further details can be found in the supplement.

4 Discussion

One additional source of uncertainty is the "tuning" of the model setups: Depending on the choice of the convection scheme several parameters in the model setup can be used to "tune" the radiation balance (and also the precipitation) to achieve realistic behaviour, which is in agreement with observations. In this study, this tuning was done only within the convection parameterisation in terms of the convective relaxation time and the convective precipitation formation rate (i.e., the conversion rate of convective cloud water into precipitation). Additionally, the entrainment and detrainment rates for the individual convection schemes are selected in agreement with recommendations from their authors. This partly explains why the convective mass fluxes and consequently the tracer distributions show such a strong dependence on the selected convection scheme.

Since the conversion of cloud water to precipitation not only determines the total rainfall, but also the energy budget within the cloud, the temperature profiles are affected, e.g. the more cloud water is transformed into precipitation that falls out of the cloud immediately, the less energy is required to evaporate the rest of the cloud (i.e., the evaporative cooling is smaller). Furthermore, decreasing the amount of condensed water decreases the moist static energy, and consequently stabilises the atmosphere. Both of these stabilising effects consequently further decrease convective activity.

Entrainment and detrainment rates are crucial for the strength of the mass fluxes, since an overestimated entrainment causes a large mass of air to be lifted, but decreases the buoyancy compared to the surroundings, consequently preventing very

ACPD
9, 11005–11050, 2009

deep convection. A weak entrainment allows deeper convection, but only with a relatively small total amount of air moved, resulting in weak mixing in the global model column. Detrainment must be considered as well: a strong detrainment in the mid troposphere prevents very deep convection and vice versa. However, even though a large degree of freedom for these processes exists (actually they even exist using only one scheme and using different parameters for entrainment, detrainment, etc., see for instance Ott et al., 2008) still climatologically realistic fields for radiation, precipitation, moisture and temperature can be achieved, as well as for the treatment of tracer transport, e.g., a bulk versus a plume ensemble transport formulation Lawrence and Rasch (2005), then this is a motivation for this study.

Since the overall effects of deep convection and the differences between the simulations are relatively large, the question of how to proceed on this issue arises. However, due to the complexity of the system a traceback to the original causes for each individual difference is difficult, and can only be attempted by the analysis of different compounds with various characteristics such as chemical reactivity and lifetime, solubility, and source distribution. A potential solution for the detailed process analysis would be a comparable study in a single column model under well defined prescribed input/boundary conditions. Nevertheless, some parts of the parameterisations are quite complex by themselves, e.g., convective microphysics, so that even in such a study a variety of results that are difficult to interpret is likely. Since in the global atmosphere a large variety of possible atmospheric conditions occur (i.e., a large selection of potentially convectively active regions (or model grid boxes) with different states of the atmosphere), global modelling studies are much better suited to capture all of these features. Furthermore, only when analysing whole regions observed conditions can be compared with the simulation results.

Since computer models of the atmospheric chemistry are usually highly non-linear (diffusion, chemistry, feedbacks, sink processes), very small deviations between simulations can easily be enhanced by the model equations resulting in larger differences. Therefore, some of the differences analysed in the sections above, e.g., those in

ACPD
9, 11005–11050, 2009

the range of ≈5%, are not necessarily completely caused by the different convection schemes, but by these non-linearities. However, for some compounds much larger variability in dependence of the convection schemes has been detected, which cannot be attributed alone to these causes. Furthermore, since all model simulations have been "pushed" towards the ECMWF reanalysis, the differences in the synoptic scale weather phenomena are small.

One important aspect to point out is that it is not the intention of this study to rate any of the schemes according to their performance, but to point out the uncertainty resulting from just one of the physical parameterisations in an atmospheric chemistry GCM. A rating is only possible with respect to observations, which will be addressed in an accompanying publication. For such a purpose the correct location, timing and intensity of convective activity must be captured by the individual convection schemes. Likely, such a success will differ from situation to situation, one being captured better by one scheme, another by another parameterisation. Furthermore, since for some compounds the distribution appears more realistic than for others with one selected parameterisation this is likely to be different for different species. Due to compensating errors/uncertainties and non-linearities not all of the effects can be easily transformed from one compound or one cause to the next. Additionally, not all of the cause-effect relationships can be readily revealed. These aspects are investigated in the accompanying paper.

5 Conclusions

In this study, it has been shown that the choice of the convection parameterisation in a global model of the chemical composition of the atmosphere can have a substantial influence on trace gas distributions. Five different state-of-the-art convection schemes have been used in an atmospheric chemistry GCM ("nudged" by the same large-scale meteorology) and the resulting trace gas distributions have been compared. A rating of performance of the schemes is not intended, but the main goal, i.e., to analyse the uncertainty for the process of parameterised convection on trace gases has been

ACPD
9, 11005–11050, 2009

determined. Depending on the atmospheric lifetime and the relevant processes for a specific compound, the differences can be up to ±100% (not necessarily of that magnitude for all species, e.g., for O_3 and CO the maximum uncertainty is globally less than ±25%, but even for these gases can locally even exceed a deviation of +100%).

The reasons for the differences are to be found both in meteorology, i.e., varying intensity and frequency of convective events, and in chemistry, i.e., precursors are affected differently by the convection due to solubility, reaction partners and location where the chemical reactions take place. Chemical and meteorological effects cannot be easily separated, so the only way to address meteorological effects alone is by using chemically inactive tracers such as ^{222}Rn. An additional important meteorological effect determined by the convection scheme is the formation of cloud and rain water and subsequent redistribution and removal of constituents from the atmosphere by precipitation scavenging. This is of larger importance for soluble compounds, but can also have a substantial effect on other species due to precursor interactions and removal. The role of water vapour as source for OH is also relevant, since higher moisture affects the oxidation capacity of the atmosphere and consequently has an influence on almost all chemical compounds. Overall, convection parameterisations are a large source of uncertainty, as well known in the community; in this study we have made an important step towards quantifying these uncertainties.

Acknowledgements. We thank J. Lelieveld for the support in performing this study. We wish to acknowledge the use of the Ferret program for analysis and graphics in this paper. Ferret is a product of NOAA's Pacific Marine Environmental Laboratory. (Information is available at http://ferret.pmel.noaa.gov/Ferret/). Furthermore, we thank the DKRZ for their support and the possibility to perform the calculations on computing devices maintained by this institution. Additionally we thank all MESSy developers and users for their support, hints, proposals and discussions. This work has been partly performed within the ENIGMA project, funded by the Max Planck society.

The service charges for this open access publication have been covered by the Max Planck Society.

References

Arakawa, A.: The Cumulus Parameterization Problem: Past, Present, and Future, J. Climate, 17, 2493–2525, 2004. 11007

Arakawa, A. and Schubert, W. H.: Interaction of a Cumulus Cloud Ensemble with the Large-Scale Environment, Part I, J. Atmos. Sci., 31, 674–701, 1974. 11007

Bechtold, P., Bazile, E., Guichard, F., Mascart, P., and Richard, E.: A mass-flux convection scheme for regional and global models, Q. J. Roy. Meteor. Soc., 127, 869–886, 2001. 11007, 11040

Bechtold, P., Chaboureau, J.-P., Beljaars, A., Betts, A. K., Köhler, M., Miller, M., and Redelsperger, J.-L.: The simulation of the diurnal cycle of convective precipitation over land in a global model, Q. J. Roy. Meteor. Soc., 130, 3119–3137, 2004. 11040

Doherty, R. M., Stevenson, D. S., Collins, W. J., and Sanderson, M. G.: Influence of convective transport on tropospheric ozone and its precursors in a chemistry-climate model, Atmos. Chem. Phys., 5, 3205–3218, 2005, http://www.atmos-chem-phys.net/5/3205/2005/. 11008, 11028

Donner, L. J., Seman, C. J., Hemler, R. S., and Fan, S.: A Cumulus Parameterization Including Mass Fluxes, Convective Vertical Velocities, and Mesoscale Effects: Thermodynamic and Hydrological Aspects in a General Circulation Model, J. Climate, 14, 3444–3463, 2001. 11007

Emanuel, K. A. and Zivkovic-Rothman, M.: Development and Evaluation of a Convection Scheme for Use in Climate Models, J. Atmos. Sci., 56, 1766–1782, 1999. 11007, 11040

Hack, J. J.: Parameterization of moist convection in the National Center for Atmospheric Research community climate model (CCM2), J. Geophys. Res., 99, 5551–5568, 1994. 11007, 11013, 11040

Jacob, D. J. and Prather, M. J.: Radon-222 as a test of convective transport in a general circulation model, Tellus, 42B, 118–134, 1990. 11016

Jöckel, P.: Technical note: Recursive rediscretisation of geo-scientific data in the Modular Earth Submodel System (MESSy), Atmos. Chem. Phys., 6, 3557–3562, 2006, http://www.atmos-chem-phys.net/6/3557/2006/. 11039

Jöckel, P., Sander, R., Kerkweg, A., Tost, H., and Lelieveld, J.: Technical Note: The Modular Earth Submodel System (MESSy) – a new approach towards Earth System Modeling, Atmos. Chem. Phys., 5, 433–444, 2005, http://www.atmos-chem-phys.net/5/433/2005/. 11008

ACPD

9, 11005–11050, 2009

Jöckel, P., Tost, H., Pozzer, A., Brühl, C., Buchholz, J., Ganzeveld, L., Hoor, P., Kerkweg, A., Lawrence, M. G., Sander, R., Steil, B., Stiller, G., Tanarhte, M., Taraborrelli, D., van Aardenne, J., and Lelieveld, J.: The atmospheric chemistry general circulation model ECHAM5/MESSy1: consistent simulation of ozone from the surface to the mesosphere, Atmos. Chem. Phys., 6, 5067–5104, 2006, http://www.atmos-chem-phys.net/6/5067/2006/. 11026, 11028, 11039

Jöckel, P., Kerkweg, A., Buchholz-Dietsch, J., Tost, H., Sander, R., and Pozzer, A.: Technical Note: Coupling of chemical processes with the Modular Earth Submodel System (MESSy) submodel TRACER, Atmos. Chem. Phys., 8, 1677–1687, 2008, http://www.atmos-chem-phys.net/8/1677/2008/. 11039

Kerkweg, A., Buchholz, J., Ganzeveld, L., Pozzer, A., Tost, H., and Jöckel, P.: Technical Note: An implementation of the dry removal processes DRY DEPosition and SEDImentation in the Modular Earth Submodel System (MESSy), Atmos. Chem. Phys., 6, 4617–4632, 2006a, http://www.atmos-chem-phys.net/6/4617/2006/. 11039

Kerkweg, A., Sander, R., Tost, H., and Jöckel, P.: Technical note: Implementation of prescribed (OFFLEM), calculated (ONLEM), and pseudo-emissions (TNUDGE) of chemical species in the Modular Earth Submodel System (MESSy), Atmos. Chem. Phys., 6, 3603–3609, 2006, http://www.atmos-chem-phys.net/6/3603/2006/. 11039

Kerkweg, A., Jöckel, P., Pozzer, A., Tost, H., Sander, R., Schulz, M., Stier, P., Vignati, E., Wilson, J., and Lelieveld, J.: Consistent simulation of bromine chemistry from the marine boundary layer to the stratosphere – Part 1: Model description, sea salt aerosols and pH, Atmos. Chem. Phys., 8, 5899–5917, 2008, http://www.atmos-chem-phys.net/8/5899/2008/. 11039

Kuo, H. L.: Further Studies of the Parameterization of the Influence of Cumulus Convection on Large-Scale Flow, J. Atmos. Sci., 31, 1232–1240, 1974. 11007

Lawrence, M. G. and Rasch, P. J.: Tracer transport in deep convective updrafts: plume ensemble versus bulk formulations, J. Atmos. Sci., 62, 2880–2894, 2005. 11009, 11031

Lawrence, M. G. and Salzmann, M.: On interpreting studies of tracer transport by deep cumulus convection and its effects on atmospheric chemistry, Atmos. Chem. Phys., 8, 6037–6050, 2008, http://www.atmos-chem-phys.net/8/6037/2008/. 11008

Lawrence, M. G., von Kuhlmann, R., Salzmann, M., and Rasch, P. J.: The balance of effects of deep convective mixing on tropospheric ozone, Geophys. Res. Lett., 30, 1940, doi:10.129/2003GL017644, 2003. 11007, 11028

ACPD

9, 11005–11050, 2009

Lelieveld, J. and Crutzen, P. J.: Role of Deep Cloud convection in the Ozone Budget of the Troposphere, Science, 264, 1759–1761, 1994. 11007, 11028

Lelieveld, J., Brhl, C., Jöckel, P., Steil, B., Crutzen, P. J., Fischer, H., Giorgetta, M. A., Hoor, P., Lawrence, M. G., Sausen, R., and Tost, H.: Stratospheric dryness: model simulations and satellite observations, Atmos. Chem. Phys., 7, 1313–1332, 2007, http://www.atmos-chem-phys.net/7/1313/2007/. 11013

Lin, J. W.-B. and Neelin, J. D.: Considerations for Stochastic Convective Parameterization, J. Atmos. Sci., 59, 959–975, 2002. 11007

Lohmann, U. and Roeckner, E.: Design and performance of a new cloud microphysics scheme developed for the ECHAM general circulation model, Clim. Dynam., 12, 557–572, 1996. 11039

Mahowald, N. M., Rasch, P. J., Eaton, B. E., Whittlestome, S., and Prinn, R. G.: Transport of ^{222}radon to the remote troposphere using the Modell of Atmospheric Transport and Chemistry and assimilated winds from ECMWF and the National Center for Environmental Prediction/NCAR, J. Geophys. Res., 102, 28139–28151, 1997. 11008

Nober, F. J. and Graf, H. F.: A new convective cloud field model based on principles of self-organisation, Atmos. Chem. Phys., 5, 2749–2759, 2005, http://www.atmos-chem-phys.net/5/2749/2005/. 11007

Nordeng, T. E.: Extended versions of the convective parametrization scheme at ECMWF and their impact on the mean and transient activity of the model in the tropics, Tech. Rep. 206, ECWMF, 1994. 11009, 11040

Ott, L., Pawson, S., and Bacmeister, J.: Quantifying the role of convection and other transport processes in determining CO distribution in the free troposphere, in: IGAC conference, 2008. 11031

Pozzer, A., Jöckel, P., Sander, R., Williams, J., Ganzeveld, L., and Lelieveld, J.: Technical Note: The MESSy-submodel AIRSEA calculating the air-sea exchange of chemical species, Atmos. Chem. Phys., 6, 5435–5444, 2006, http://www.atmos-chem-phys.net/6/5435/2006/. 11039

Pozzer, A., Jöckel, P., Tost, H., Sander, R., Ganzeveld, L., Kerkweg, A., and Lelieveld, J.: Simulating organic species with the global atmospheric chemistry general circulation model ECHAM5/MESSy1: a comparison of model results with observations, Atmos. Chem. Phys., 7, 2527–2550, 2007, http://www.atmos-chem-phys.net/7/2527/2007/. 11022, 11024

Price, C., Penner, J., and Prather, M.: NO_x from lightning, 1. Global distribution based on

lightning physics, J. Geophys. Res., 102, 5929–5941, 1997. 11009
Roeckner, E., Bäuml, G., Bonaventura, L., Brokopf, R., Esch, M., Giorgetta, M., Hagemann, S., Kirchner, I., Kornblue, L., Manzini, E., Rhodin, A., Schleese, U., Schulzweida, U., and Tompkins, A.: The atmospheric general circulation model ECHAM5: Part 1, Tech. Rep. 349, Max-Planck-Institut für Meteorologie, 2003. 11039
Roeckner, E., Brokopf, R., Esch, M., Giogetta, M., Hagemann, S., Kornblueh, L., Manzini, E., Schleese, U., and Schulzweida, U.: Sensitivity of simulated climate to horizontal and vertical resolution in the ECHAM5 atmosphere model, J. Climate, 19, 3771–3791, 2006. 11008
Sander, R., Kerkweg, A., Jöckel, P., and Lelieveld, J.: Technical note: The new comprehensive atmospheric chemistry module MECCA, Atmos. Chem. Phys., 5, 445–450, 2005, http://www.atmos-chem-phys.net/5/445/2005/. 11039
Tabazadeh, A., Toon, O. B., and Jensen, E. J.: A surface chemistry model for nonreactive trace gas adsorption on ice: Implications for nitric acid scavenging by cirrus, Geophys. Res. Lett., 26, 2211–2214, 1999. 11011
Tiedtke, M.: A Comprehensive Mass Flux Scheme for Cumulus Parametrization in Large-Scale Models, Mon. Weather Rev., 117, 1779–1800, 1989. 11007, 11009, 11040
Tost, H.: Global Modelling of Cloud, Convection and Precipitation Influences on Trace Gases and Aerosols, Ph.D. thesis, Rheinische Friedrich-Wilhelms-Universität Bonn, Germany, available at: http://hss.ulb.uni-bonn.de/diss_online/math_nat_fak/2006/tost_holger, 2006. 11009, 11016
Tost, H., Jöckel, P., Kerkweg, A., Sander, R., and Lelieveld, J.: Technical note: A new comprehensive SCAVenging submodel for global atmospheric chemistry modelling, Atmos. Chem. Phys., 6, 565–574, 2006a, http://www.atmos-chem-phys.net/6/565/2006/. 11010, 11039
Tost, H., Jöckel, P., and Lelieveld, J.: Influence of different convection parameterisations in a GCM, Atmos. Chem. Phys., 6, 5475–5493, 2006b, http://www.atmos-chem-phys.net/6/5475/2006/. 11007, 11009, 11011, 11013, 11014, 11015, 11016, 11028, 11039
Tost, H., Jöckel, P., Kerkweg, A., Pozzer, A., Sander, R., and Lelieveld, J.: Global cloud and precipitation chemistry and wet deposition: tropospheric model simulations with ECHAM5/MESSy1, Atmos. Chem. Phys., 7, 2733–2757, 2007a, http://www.atmos-chem-phys.net/7/2733/2007/. 11030, 11039
Tost, H., Jöckel, P., and Lelieveld, J.: Lightning and convection parameterisations – uncertainties in global modelling, Atmos. Chem. Phys., 7, 4553–4568, 2007b,

http://www.atmos-chem-phys.net/7/4553/2007/. 11007, 11009, 11039
von Kuhlmann, R. and Lawrence, M. G.: The impact of ice uptake of nitric acid on atmospheric chemistry, Atmos. Chem. Phys., 6, 225–235, 2006, http://www.atmos-chem-phys.net/6/225/2006/. 11011
Vignati, E., Wilson, J., and Stier, P.: M7: An efficient size-resolved aerosol microphysics module for large-scale aerosol transport models, J. Geophys. Res., 109, D22202, doi: 10.1029/2003JD004485, 2004. 11039
Wilcox, E. M.: Spatial and Temporal Scales of Precipitation Tropical Cloud Systems in Satellite Imagery and the NCAR CCM3, J. Climate, 16, 3545–3559, 2003. 11040
Xie, P. and Arkin, P.: Global Precipitation: A 17-year Monthly Analysis Based on Gauge Observations, Satellite Estimates and Numerical Model Outputs, B. Am. Meteorol. Soc., 78, 2539–2558, 1997. 11025
Zhang, G. J. and McFarlane, N. A.: Sensitivity of Climate Simulations to the Parameterization of Cumulus Convection in the Canadian Climate Centre General Circulation Model, Atmos.-Ocean, 33, 407–446, 1995. 11007, 11040
Zhang, K., Wan, H., Zhang, M., and Wang, B.: Evaluation of the atmospheric transport in a GCM using radon measurements: sensitivity to cumulus convection parameterization, Atmos. Chem. Phys., 8, 2811–2832, 2008, http://www.atmos-chem-phys.net/8/2811/2008/. 11008, 11019

Table 1. Applied processes and respective submodels of EMAC.

Process	Submodel name	Reference
Air sea exchange of trace species	AIRSEA	Pozzer et al. (2006)
Large-scale condensation	CLOUD	see Lohmann and Roeckner (1996) Roeckner et al. (2003)
Convection	CONVECT	Tost et al. (2006b)
Convective tracer transport	CVTRANS	see below
^{222}Rn cycle	DRADON	P. Jöckel (unpublished)
Dry deposition	DRYDEP	Kerkweg et al. (2006a)
H_2O chemical tendency	H2O	see Jöckel et al. (2006)
Photolysis	JVAL	see Jöckel et al. (2006)
Lightning NO_x emissions	LNOX	Tost et al. (2007b)
Aerosol microphysics	M7	see Vignati et al. (2004) Kerkweg et al. (2008)
Gas phase chemistry	MECCA	Sander et al. (2005)
Emissions and other boundary conditions	OFFLEM, ONLEM, TNUDGE NCREGRID	Kerkweg et al. (2006b) Jöckel (2006)
Prognostic tracers	TRACER, PTRAC	Jöckel et al. (2008)
QBO nudging	QBO	Jöckel et al. (2006)
Radiation	RAD4ALL	see Jöckel et al. (2006)
Scavenging and cloud/precipitation chemistry	SCAV	Tost et al. (2006a) Tost et al. (2007a)
Aerosol sedimentation	SEDI	Kerkweg et al. (2006a)
Tropopause diagnostics	TROPOP	Jöckel et al. (2006)
Diagnostic tools for the output	various submodels	P. Jöckel (unpublished)

ACPD
9, 11005–11050, 2009

Table 2. Convection schemes in the individual simulations.

Simulation name	description and references
T1	Tiedtke (1989) with modifications of Nordeng (1994)
EC	IFS cycle 29r1b from the ECMWF (Bechtold et al., 2004)
EMA	Emanuel and Zivkovic-Rothman (1999)
ZHW	Zhang and McFarlane (1995) and Hack (1994) with a modification from Wilcox (2003)
B1	Bechtold et al. (2001)

Table 3. 4 month average of the upper tropospheric ^{222}Rn burden (in g) from the 500 hPa level to the tropopause and the fraction of the total radon burden (in %).

Simulation	Burden	Fraction of total burden above 500 hPa
T1	34.8	16.7
EC	36.8	17.3
Ema	33.4	16.0
ZHW	34.7	16.5
B1	47.1	22.6

ACPD

9, 11005–11050, 2009

Table 4. 4 month average of the tropospheric O_3 burden (in Tg) from the surface to the tropopause.

Simulation	Burden
T1	331.7
EC	318.8
Ema	324.5
ZHW	328.6
B1	342.1

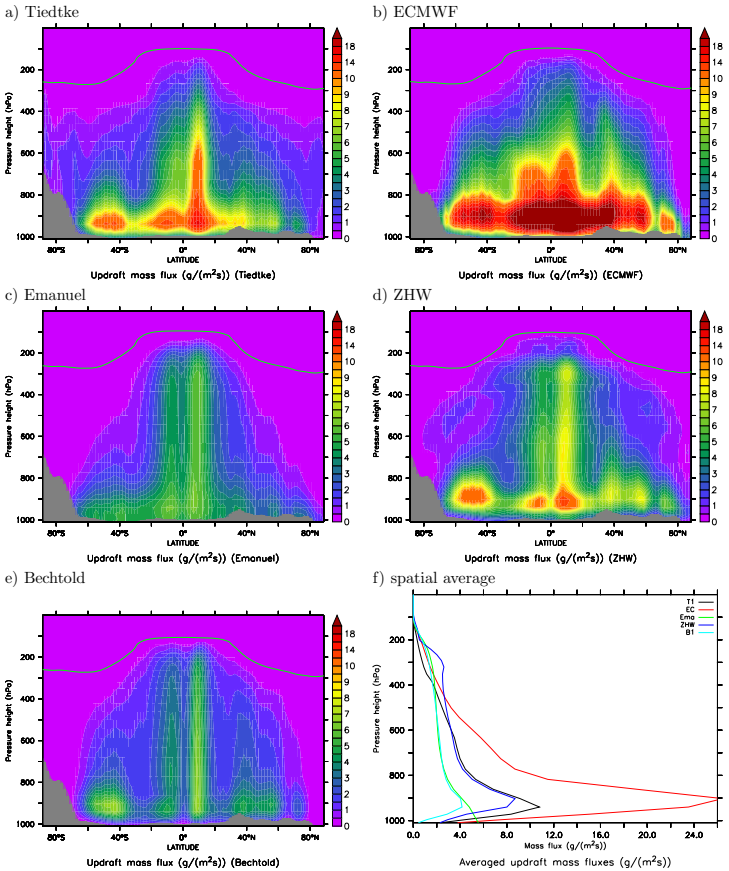

Fig. 1. 4 months average (September–December 2005) of the zonal averaged convective updraft mass fluxes **(a–e)** in g/(m^{2}s) and average vertical profile **(f)**. The green line denotes the tropopause and the grey shaded area the zonal mean orography.

ACPD
9, 11005–11050, 2009

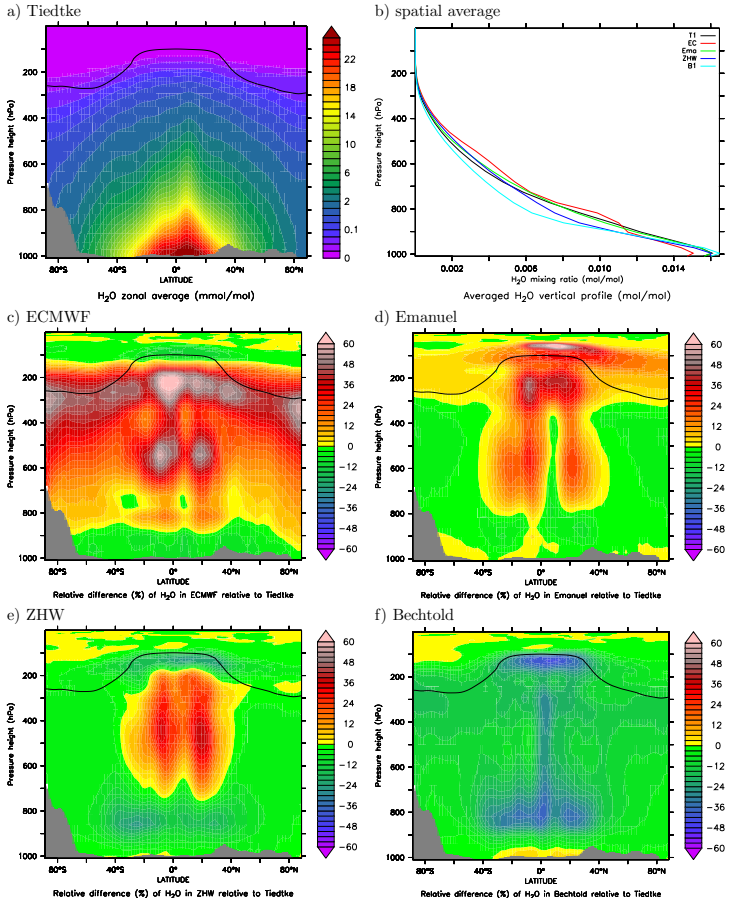

Fig. 2. 4 months average of the zonal mean H_2O in nmol/mol **(a)**, and the average vertical profile (nmol/mol) in the five simulations **(b)**. Panels **(c)** to **(f)** show the relative differences (in %) with Tiedtke as reference: $((X-T1)/T1 \cdot 100)$. The black line denotes the tropopause and the grey shaded area the zonal mean orography.

ACPD
9, 11005–11050, 2009

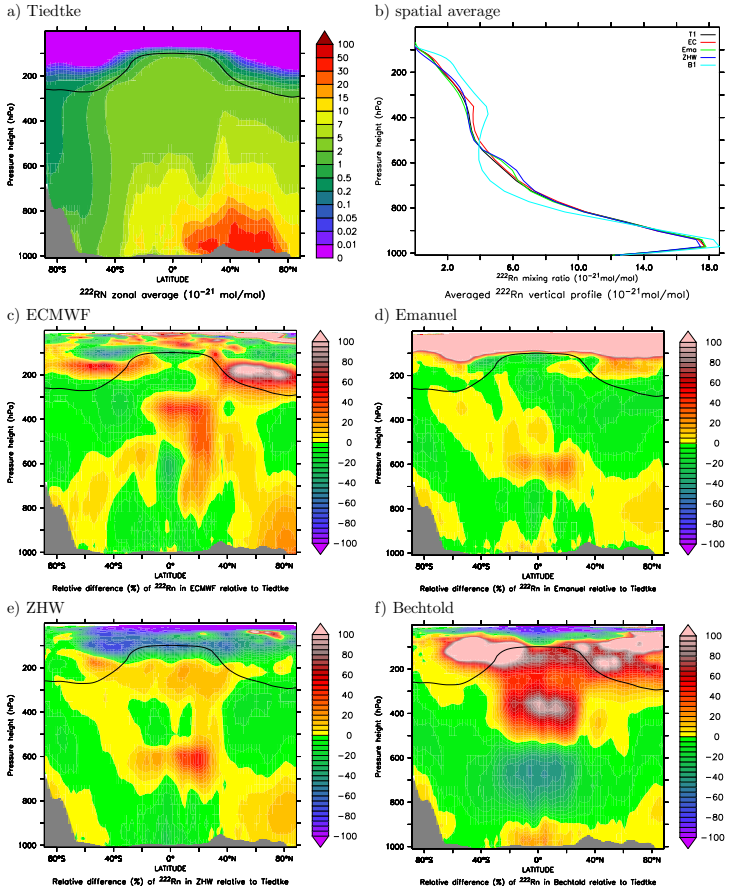

Fig. 3. 4 month average of the zonal mean ^{222}Rn (in nmol/mol) **(a)**, and the average vertical profile (nmol/mol) in the five simulations **(b)**. Panels **(c)** to **(f)** depict the relative differences (in %) with Tiedtke as the reference: $((X-T1)/T1 \cdot 100)$. The black line denotes the tropopause and the grey shaded area the zonal mean orography.

ACPD
9, 11005–11050, 2009

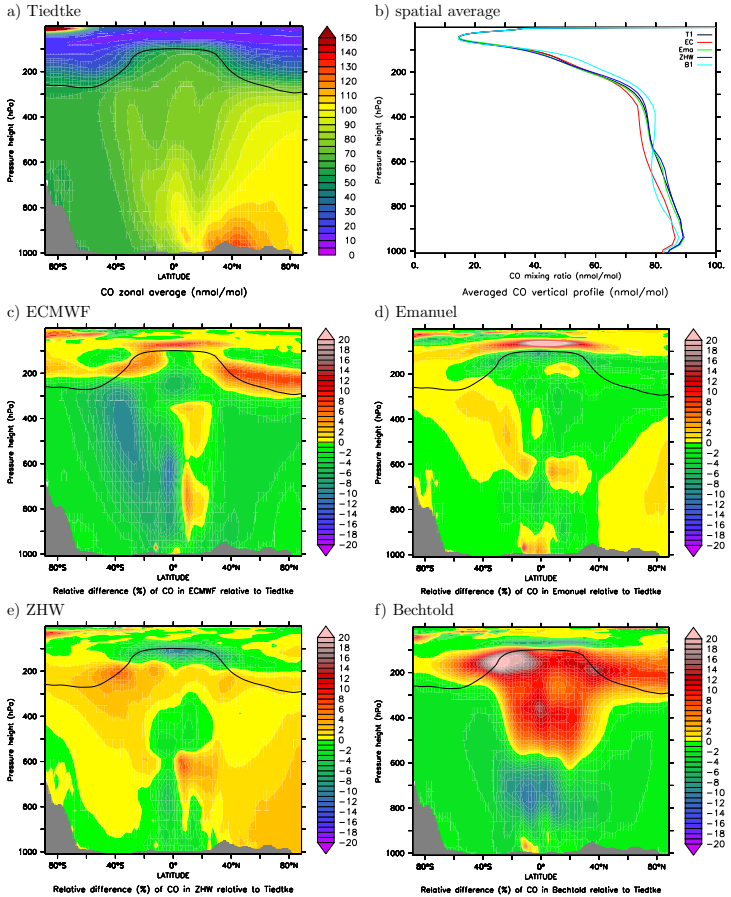

Fig. 4. 4 months average of the zonal mean CO (in nmol/mol) **(a)**, and the average vertical profile (nmol/mol) in the five simulations **(b)**. Panels **(c)** to **(f)** depict the relative differences (in %) with Tiedtke as the reference: $((X-T1)/T1 \cdot 100)$. The black line denotes the tropopause and the grey shaded area the zonal mean orography.

ACPD
9, 11005–11050, 2009

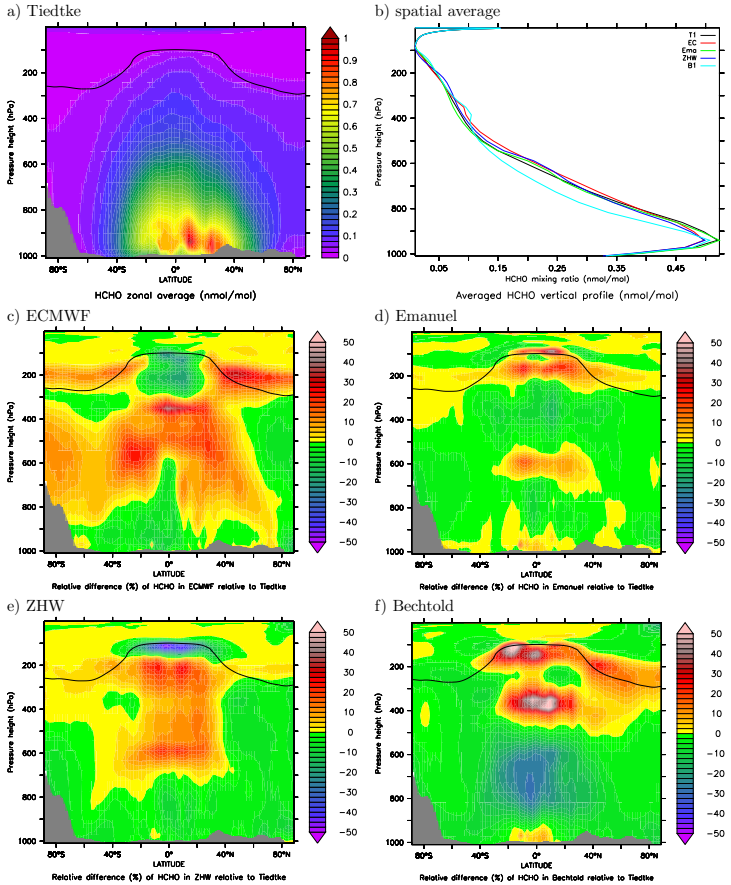

Fig. 5. 4 month average of the zonal mean HCHO (in nmol/mol) **(a)**, and the average vertical profile (in nmol/mol) in the five simulations **(b)**. Panels **(c)** to **(f)** depict the relative differences (in %) with Tiedtke as the reference: $((X - T1)/T1 \cdot 100)$. The black line denotes the tropopause and the grey shaded area the zonal mean orography.

ACPD
9, 11005–11050, 2009

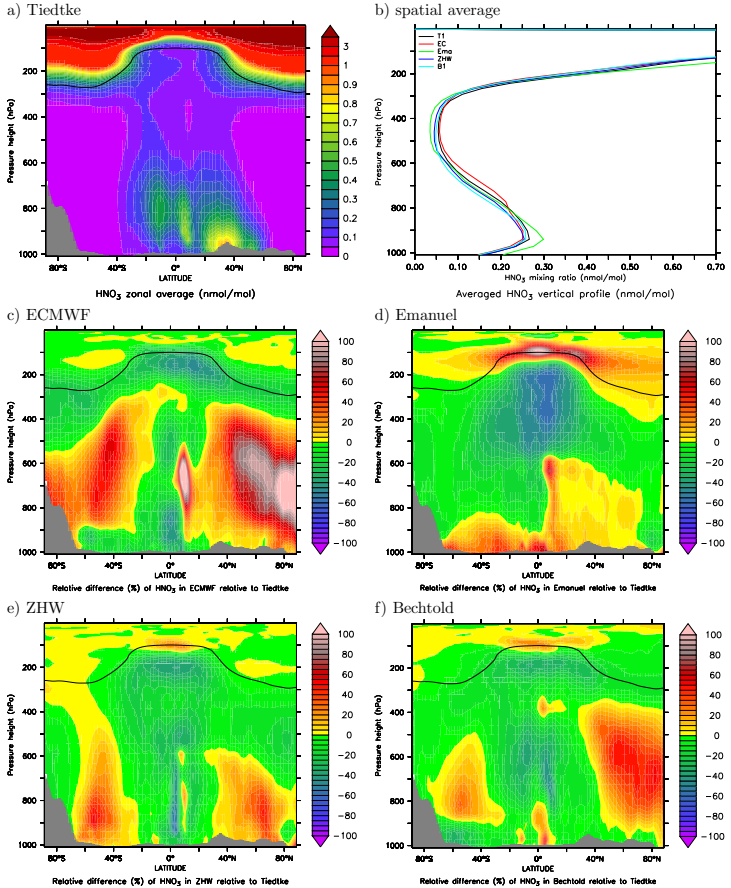

Fig. 6. 4 month average of the zonal mean HNO_3 (in nmol/mol) **(a)**, and the average vertical profile (in nmol/mol) in the five simulations **(b)**. Panels **(c)** to **(f)** depict the relative differences (in %) with Tiedtke as the reference: $((X-T1)/T1 \cdot 100)$. The black line denotes the tropopause and the grey shaded area the zonal mean orography.

ACPD
9, 11005–11050, 2009

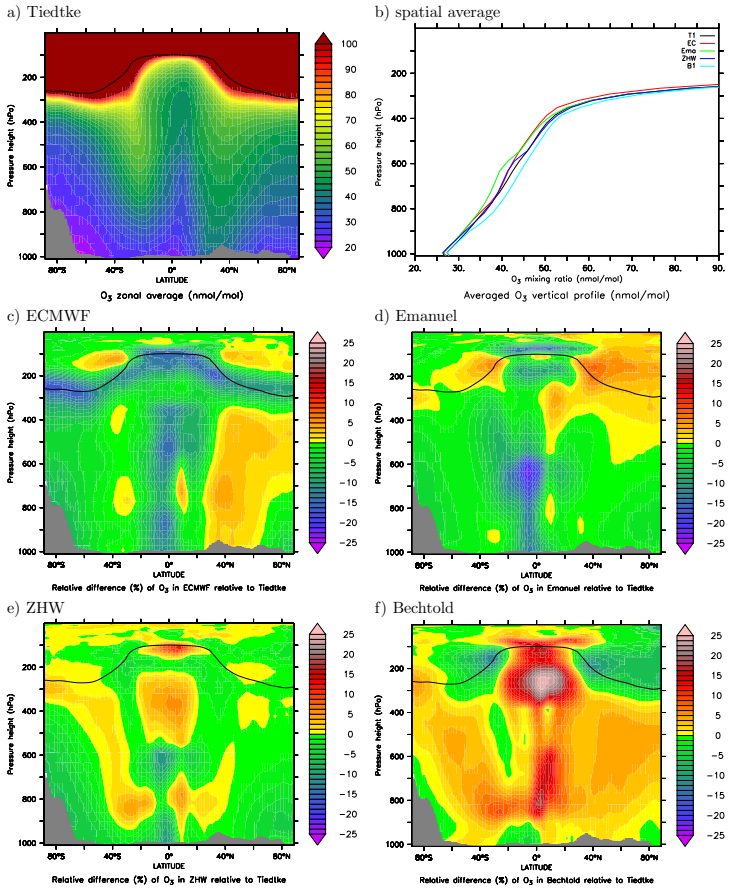

Fig. 7. 4 months average of the zonal mean O_3 (in nmol/mol) **(a)**, and the average vertical profile (in nmol/mol) in the five simulations **(b)**. Panels **(c)** to **(f)**) depict the relative differences (in %) with Tiedtke as the reference: $((X - T1)/T1 \cdot 100)$. The black line denotes the tropopause and the grey shaded area the zonal mean orography.

ACPD
9, 11005–11050, 2009

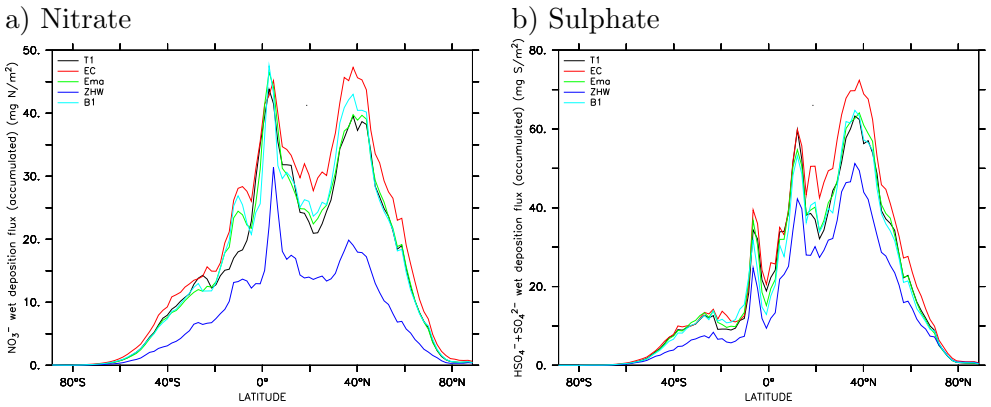

Fig. 8. Accumulated zonally averaged nitrate **(a)** and sulphate **(b)** wet deposition flux (each in mg N or S per m^2) at the surface. The different colours denote the different simulations.

ACPD
9, 11005–11050, 2009